arXiv:1612.07981v1 [cond-mat.mtrl-sci] 23 Dec 2016

Density functional theory study of vacancy induced magnetism in Li_3N

A. Östlin[1] and L. Chioncel[1,2]

[1] *Theoretical Physics III, Center for Electronic Correlations and Magnetism, Institute of Physics, University of Augsburg, D-86135 Augsburg, Germany*

[2] *Augsburg Center for Innovative Technologies, University of Augsburg, D-86135 Augsburg, Germany*

Abstract

The effect of lithium vacancies in the hexagonal structure of $\alpha-Li_3N$, is studied within the framework of density functional theory. Vacancies ($\square$) substituting for lithium in $\alpha-Li_2(Li_{1-x}\square_x)N$ are treated within the coherent potential approximation as alloy components. According to our results long range N(p)-ferromagnetism ($\sim 1\ \mu_B$) sets in for vacancy substitution within the [Li_2N] layers ($x \geq 0.7$) with no significant change in unit cell dimensions. By total energies differences we established that in-plane exchange couplings are dominant. Vacancies substituting inter-plane Li, leads to a considerable structural collapse ($c/a \approx 0.7$) and no magnetic moment formation.

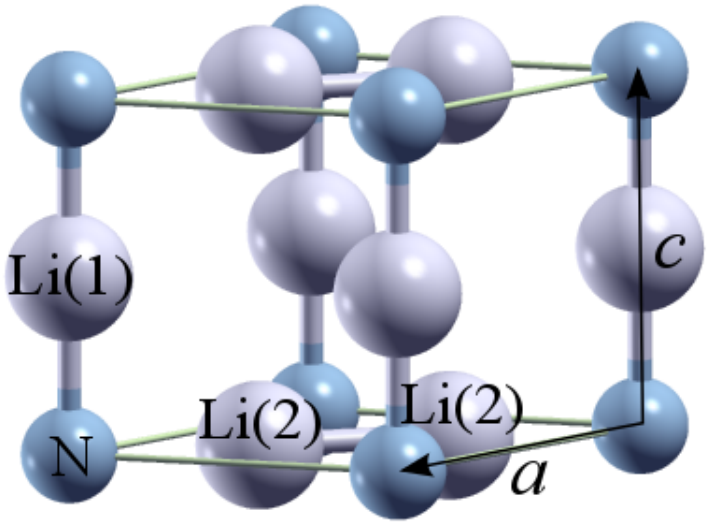

FIG. 1: Crystal structure of $\alpha-Li_3N$. The crystal is made of hexagonally close-packed layers of Li_2N, where the Li atoms are denoted by Li(2). These layers are alternated by Li layers, where the Li is denoted by Li(1). The Li(1) atom is placed inbetween the N in the Li_2N layers.

I. INTRODUCTION

Lithium nitride (Li_3N) is the only known stable alkali metal nitride. At ambient conditions it crystallizes in the hexagonal $P6/mmm$ structure ($\alpha-Li_3N$) seen in Fig. 1. The structure consists of alternating Li and Li_2N layers [1, 2]. The basal ab-plane contains edge sharing planar Li hexagons centred by nitrogen. These planes are connected through a further lithium ion along the c-axis located directly on top of the N. Each nitrogen is coordinated by eight lithium atoms in a hexagonal bipyramid geometry. Within the Li_2N layers (ab-planes) the atoms are close-packed, while the Li layers form an open structure. In the following the Li above the N atom will be denoted as Li(1) and the Li atoms within the Li_2N layers will be denoted as Li(2), see Fig. 1. It is known that the bonding in this material is mainly ionic, with the three lithium atoms donating their $2s$ electrons to the nitrogen, resulting in Li^+ ions and a N^{3-} ion [3]. Lithium nitride is a common material used in the solid-state battery technology [2, 4]: the indirect band gap is about 2.1 eV [5] and the material has exceptionally high Li^+ ion mobility [2], which arises from the cationic vacancies within the [Li_2N] planes.

Sachsze and Juza [6] found that the Li(1) atom could easily be substituted by a transition

metal atom. This possibility has recently generated a substantial amount of interest due to the large magnetic moment observed at the substituted site [7–11]. This magnetic moment supersedes that of the donor transition metal element and is attributed to the absence of orbital moment quenching and to on-site Coulomb interactions [9]. These findings have led to predictions that transition metal doped Li_3N might be considered for replacing rare-earth permanent magnets [10]. The magnetic behaviour associated with the presence of transition metal atoms lead us to raise the question if magnetism is still triggered if non-magnetic atoms, or in the extreme case vacancies, are used as dopants in the structure of lithium nitride. In the present paper the effect of vacancy induced magnetism is studied theoretically using density functional theory (DFT) [12–14] methods.

The electronic structure of the ordered $\alpha-Li_3N$ crystal has been studied using density functional [15–17] and Hartree-Fock [18, 19] theories. Similar studies has been performed on the Li ion vacated structure [20], also using molecular dynamics [17]. None of these calculations took the spin-polarization of the charge density into account, and therefore magnetic effects were not reported previously.

Besides $\alpha-Li_3N$, two other polymorphs exist: the hexagonal $\beta-Li_3N$ stable at moderate pressure (4.2 kbar and 300 K) [21, 22] and the cubic $\gamma-Li_3N$ stable up to 200 GPa [22, 23]. It has been demonstrated that Li_3N retains its ionic character through the significant structural transformation [22]. Upon pressure, the band gap is increased across the hexagonal (β) to cubic (γ) structural transition. The increase in the magnitude of the band gap is a consequence of the loss of the lowest laying conduction band as one goes from $\beta \rightarrow \gamma$ [23]. The large (5.5 eV) gap $\gamma-Li_3N$ material was found to show anomalous color, which could be due to presence of vacancies (color centres) [23]. It is commonly found that the lithium vacancy concentration increases with doping, especially at the Li(2) sites [24]. In the extreme case of LiNiN, where full substitution of the Li(1) atom with nickel has been achieved, one of the Li(2) sites is completely vacated, creating a crystal structure with the $P\bar{6}m2$ space group [25, 26]. As expected, the presence of Ni determines the magnetic properties of LiNiN. On the other hand, in the absence of the transition metal, it is obvious to ask if p-orbital magnetism can be induced due to vacancies in this system.

Magnetism is most often associated with systems containing partially occupied $d-$ or $f-$shells. In transition metals or rare earth elements, Hunds exchange energy and the kinetic energy are of similar magnitude, and magnetism may appear if the Hund energy is large

enough [27]. A similar discussion has been extended to $p-$electronic systems, containing C, N or O [28]. In order to elucidate on the effect of vacancies on total energy and magnetism, we have in this paper performed a DFT study on the electronic structure of Li_3N with Li atom vacancies. In our work we show that the creation of Li atom vacancies within the perfect $\alpha-Li_3N$ structure induces: (i) a volume collapse of a magnitude which depends on the symmetry position of the removed Li atom, and also (ii) magnetism, with moments centred on the N ions. In the case of a removal of the Li(1) atom, a large structural collapse occurs which leads to the vanishing of the magnetic moment. For removal of Li(2) atoms the volume reduction is not drastic, and a magnetic moment is still formed. We also compute the vacancy concentration needed to form long-range magnetic ordering between the vacancy-induced N-moments in this system.

The paper is organized as follows: In Section II we introduce the theoretical tools used in the study, and present the computational details. Section III first presents the calculated ground-state lattice parameters of Li_3N, and the effect of a complete removal of inter- and in-plane Li atoms. We also investigate the partial, non-stoichiometric, replacement of one of the in-plane Li atoms by a vacancy, employing the coherent potential approximation. In the second part of Section III we present the band structure of Li_3N, with and without vacancies. At the end of Section III, the ordering of the magnetic moments is discussed. Section IV provides the discussion of the results, and Section V gives a conclusion.

II. METHODOLOGY AND COMPUTATIONAL DETAILS

The electronic structures for all systems were obtained by Kohn-Sham density functional theory [12, 13]. Three different basis sets to represent the Kohn-Sham orbitals were used, namely the full-potential linearised augmented plane wave (FPLAPW) method as implemented in *elk* [29], the exact muffin-tin orbitals (EMTO) method [30–32] and the linearised muffin-tin (LMTO) method [33]. As seen from Fig. 1, Li_3N has an open structure, with large interstitial areas in the Li(1) layer planes. To model this large interstitial region, the LMTO and EMTO methods introduce so called 'empty spheres' into the structure in order to improve upon the spherical potential approximation. The full potential is taken into account in the FPLAPW method.

To model the non-stoichiometric substitution of Li atoms with vacancies, we employed

the coherent potential approximation (CPA) within the EMTO method. The EMTO-CPA method together with the full-charge density (FCD) [34] scheme has proven able to accurately determine the total energy due to anisotropic lattice distortions (e.g hexagonal c/a-ratios) for real systems with substitutional disorder [35].

For the FPLAPW calculations the plane-wave cutoff K_{max} was set so that $R_{mt}K_{max} = 8.0$, where R_{mt} is the muffin-tin radius. The radii of the muffin tins were set to $R = 1.7$ a.u. for N, $R = 1.45$ a.u. for Li(1) and $R = 1.8$ a.u. for Li(2), and were kept fixed for all volumes and c/a-ratios considered. The irreducible Brillouin zone was sampled with 333 **k**-points, and a Fermi smearing function was employed at room temperature. The N 1s-state was treated as core, while the remaining states were treated as valence. The exchange correlation potential was treated within the local density approximation (LDA) [36].

The EMTO calculations were done with a angular momentum cutoff keeping the *spd*-states. The kink-cancellation equation was solved along a semicircular contour in the complex energy plane, with the bottom at -1.5 Ry below the Fermi level. In this way the contour enclosed the N 2s semicore states. The irreducible Brillouin zone was sampled with 324 **k**-points. Empty spheres where included at the positions $(\frac{2}{3},\frac{1}{3},\frac{1}{2})$ and $(\frac{1}{3},\frac{2}{3},\frac{1}{2})$, i.e. in the same plane as Li(1) and right above the Li(2), in order to cover the interstitial volume. The energy dependence of the slope matrix was parametrized using the two-center Taylor expansion technique [37]. The volume vs. c/a-ratio total energy contours were calculated for 5 volumes and 5 c/a-ratios, and interpolation and energy minimization were performed to find the minima.

III. RESULTS AND DISCUSSION

A. Perfect Li_3N

We first optimized the volume and c/a-ratio for the perfect Li_3N. The energy landscape as given by the FPLAPW method for the volume vs. c/a-ratio can be seen in Fig. 2 (left). The FPLAPW method results in a ground-state volume of $V_0 = 278.12$ a.u.^{3} and $c/a = 1.070$, while the EMTO method gives volume of $V_0 = 276.62$ a.u.^{3} and $c/a = 1.069$. The results are in good agreement with each other, indicating that the spherical approximation is valid. Lattice optimization were also done within the FPLAPW method employing the PBE-

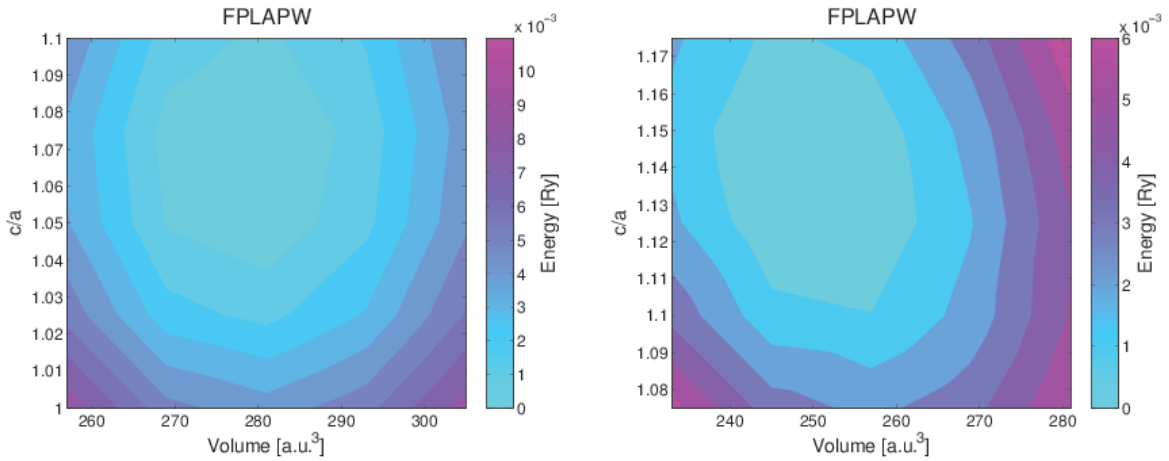

FIG. 2: Left: Volume versus c/a-ratio energy map of perfect Li_3N, calculated with the FPLAPW method. Right: Volume versus c/a-ratio energy map $Li_2(\square)N$, where the vacancy $\square$ is of type Li(2) i.e. in-plane.

GGA [38] for the exchange-correlation potential, which results in a slight increase in volume (6%) compared to the LDA result, and $c/a = 1.062$. Previous Hartree-Fock calculations have given values of $V_0 = 292.46$ a.u.^{3} and $c/a = 1.0637$ (Ref. [18]). Our results can be seen to agree well with experimental (Table I) and previous theoretical studies. Also note that the calculations predict an insulating state for Li_3N, in agreement with experiment. Spin-polarized calculations were also performed, and no magnetic moment was found. In Fig. 3 are shown contour plots of the total charge density as calculated within the EMTO method of Li_3N. The charge densities show good agreement compared to previous studies [15, 23]. Note the close packing within the Li_2N layer (left) and the large interstitial region between the layers (right).

B. Vacancies within the [Li_2N]-plane

A vacancy (denoted by $\square$) created by removing one of the (geometrically equivalent) Li(2) atoms changes the space group to $P\bar{6}m2$. If the lattice parameters from the perfect Li_3N are kept, the calculations for the Li(2) vacated structure predicts a non-zero density of states at the Fermi level, indicating that the system has turned metallic. If the spin-symmetry is broken, the system turns ferromagnetic (FM) with an integer moment of 1 μ_B. The underlying reasons for the onset of magnetization will be discussed in more detail

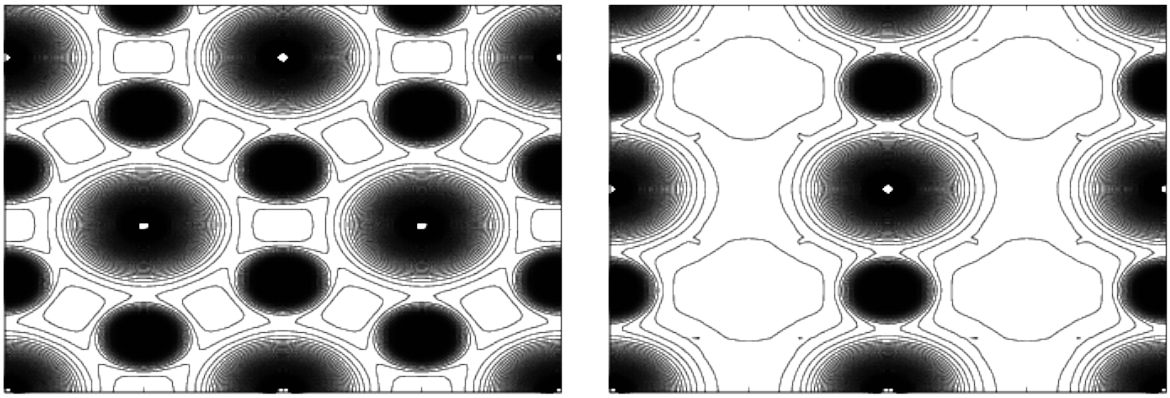

FIG. 3: Left: Total charge density for Li_3N within the *ab*-plane. Right: Total charge density for Li_3N in the (100)-plane. The contour line spacing is 0.01 in atomic units. Calculations performed at a volume close to equilibrium, $V = 281$ a.u.^{3} ($c/a = 1.05$).

TABLE I: Volumes in atomic units (first rows) and c/a-ratios (second rows) for perfect Li_3N, Li_2N (in-plane Li(2) vacancy) and $Li_2(Li_{0.5}\square_{0.5})N$ as calculated within our methods. Comparison made with experimental sources where possible.

		FPLAPW	EMTO	Ref. [3]	Ref. [10]
Li_3N	(V_0)	278.12	276.62	299.98	301.65
	(c/a)	1.070	1.069	1.0634	1.0597
Li_2N	(V_0)	248.50	252.31		
(inplane)	(c/a)	1.141	1.071		
$Li_2(Li_{0.5}\square_{0.5})N$	(V_0)		269.04		
	(c/a)		1.065		

in Sections III D and III E. To see if the removal of the Li(2) atom has any effect on the geometry of the structure we optimized the lattice parameters, see Fig. 2 (right). We found that the ground-state volume within EMTO reduces slightly to $V_0 = 252.31$ a.u.^{3}, and the c/a-ratio becomes 1.071. For the FPLAPW, we got $V_0 = 248.50$ a.u.^{3}, and the c/a-ratio becomes 1.141. The slight discrepancy in the $c/a-$ratio between the FPLAPW and EMTO methods could possibly be due to the spherical approximation used in the latter as also reported previously [39].

In Fig. 4 the total charge density in real space is plotted within the *ab*-plane, where a

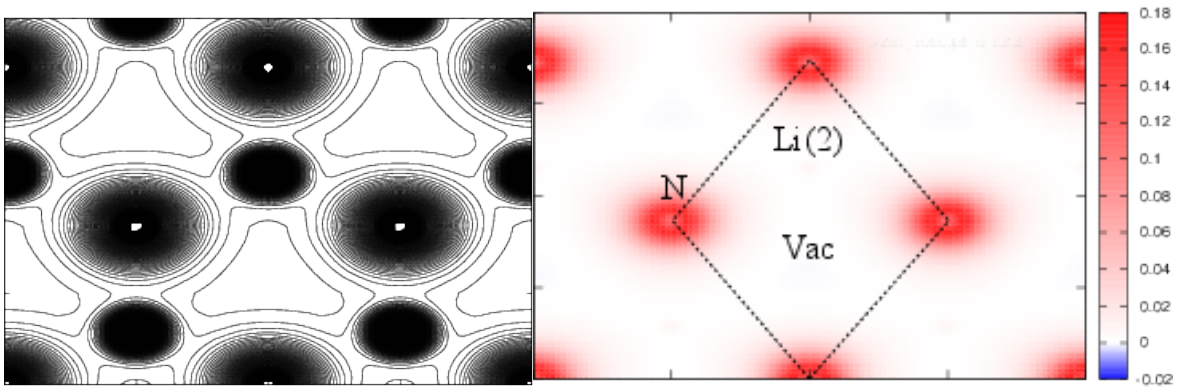

FIG. 4: Left: Total charge density $n_\uparrow(\mathbf{r}) + n_\downarrow(\mathbf{r})$ for $Li_2\square N$ in the ab-plane. Spacing between contour lines is 0.01 in atomic units. Right: Magnetization density $n_\uparrow(\mathbf{r}) - n_\downarrow(\mathbf{r})$ for $Li_2\square N$ in the ab-plane. Calculations performed at a volume close to equilibrium, $V = 281$ a.u.^{3} ($c/a = 1.05$).

comparison with the case of the perfect Li_3N structure (Fig. 3 (left)) shows the vacant Li(2) positions in the lattice. The magnetization density, defined as the difference between the real space majority and minority spin density, $n_\uparrow(\mathbf{r}) - n_\downarrow(\mathbf{r})$, is shown on the right hand-side of Fig. 4. Note that the magnetization density is sizeable mainly around the nitrogen ions, indicating that the spin density is highly localized around the nitrogen positions in real space.

In order to see how the lattice parameters change as the concentration of vacancies increases, the structural disorder was modelled using the alloy analogy within the EMTO-CPA method. In this method the vacancy is treated as an 'alloy component' represented by an empty atomic sphere. The system thus had the chemical formula $Li_2(Li_{1-x}\square_x)N$, where the vacancy is of Li(2) type. For $x = 0.5$ one-fourth of the Li(2) atoms are vacated. The results of the lattice parameter optimization performed within DFT calculations is presented in Fig. 5 (left). The equilibrium volume is $V_0 = 269.04$ a.u.^{3} and the corresponding ratio $c/a = 1.065$. The EMTO results (Table I) for the clean Li_3N gives a lattice constant $a = 3.538$ Å while an in-plane Li(2)-vacated lattice Li_2N has $a = 3.429$ Å. From these two limits we propose the following linear concentration dependence of the lattice parameter: $a(x) = 3.429 + 0.109x$ Å. For the concentration $x = 0.5$ our total energy optimization gives for the lattice parameter a the result: $a = 3.483$ Å. We note that this result agrees with the empirical Vegards-type law (linear increase of lattice constant as a function of concentration)

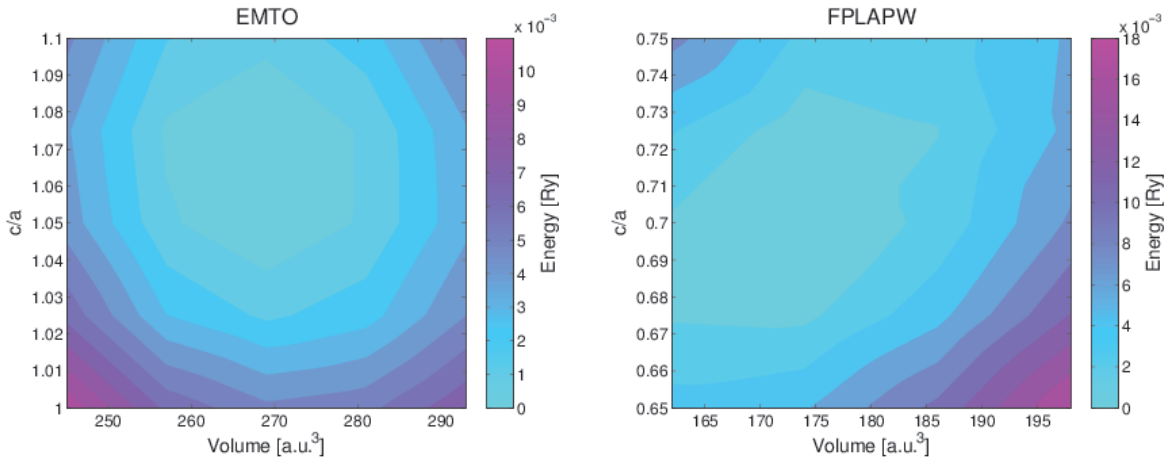

FIG. 5: Left: Volume versus c/a-ratio energy map $Li_2(Li_{0.5}\square_{0.5})N$, where the vacancy $\square$ is of type Li(2) i.e. in-plane, calculated within EMTO-CPA. Right: $Li_2(\square)N$, where the vacancy is of type Li(1) i.e. out-of-plane.

to within 1%.

C. Interplane vacancies at Li(1)-site

We next consider a full removal of the Li(1) atom, i.e. a complete removal of the Li(1)-plane. For the practical calculation this corresponds to a crystal structure model in which the Li(1)-plane consists of empty-spheres. The energy landscape for the volume vs. c/a-ratio can be seen in Fig. 5. As the Li(1) atom is removed, the crystal becomes unstable and the c/a-ratio 'collapses' to ~ 0.7. The decrease in the length of the c-axis is accompanied by a reduction in unit cell volume to around 172.61 a.u.^{3}, and consequently the spin-polarization vanishes. Due to this sizeable reduction of volume, c/a-ratio and magnetic moment, further computations with Li(1) vacancies was not carried on since it would lead to a significant departure from the structure of interest in experimental studies.

D. Band structure

Results of the band structure calculations for the systems in discussion are shown in Fig. 6. The band structure for perfect Li_3N, using the experimental lattice parameters, is seen in the top left of Fig. 6, and agrees well with previous theoretical studies [15, 23]. The three valence bands have mainly N-p orbital character, with the p_x- and p_y-states being degenerate

at certain high symmetry points/directions within the Brillouin zone. The lowest laying conduction band has mixed (sp) character, and its density is situated predominantly in the region inbetween the Li_2N layers, as shown in Ref. [23]. The gap ($\lesssim 1.5$ eV) underestimates the experimental one (~ 2.1 eV [5]), which is a common effect seen within DFT. Band structure calculations within the PBE-GGA were also performed, and no major change in bands and band gaps were found.

As a Li(2) atom is removed from the system, the N p-bands becomes partially occupied and the chemical potential readjusts to account for the number of electrons (Fig. 6, top right). The most drastic change is a spin-splitting of the bands: one spin channel being completely occupied while the opposite one is almost rigidly shifted upwards in energy. Note that only the $p_x + p_y-$orbital of the minority spin channel is shifted above the Fermi level. In Fig. 6 (bottom left) the results for the band structure for the perfect Li_3N cell with a completely removed Li(1) atom is seen. The result is similar to the case of a Li(2) vacancy, namely: one spin channel is being shifted almost rigidly upwards in energy. In the case of Li(1) vacancy, we have identified the p_z-orbital that is completely shifted above the Fermi level. In addition, the structural optimization showed that the widely separated Li_2N layers are unstable, and that the structure collapses to a smaller volume and a smaller $c/a-$ratio. The band structure for the collapsed structure is shown in Fig. 6 (bottom right). In this case, the remaining N-p_z bands acquire a broad dispersion in the $\Gamma - A$-direction, suppressing the magnetism. We also performed calculations for a pressurized system up to 20% of the lattice constants (both isotropic and $c-$axial compression), and the system remained metallic.

E. Magnetic ordering

In this section we analyse the results of the electronic structure in the view of the interplay between the magnetic moment formation and the vacancy concentration in Li_3N. In these calculations a constant volume equal to that of the Li_2N structure (252.31 a.u.^{3}) and the corresponding constant c/a-ratio equal to 1.07 were assumed.

For vacancy concentrations $x \leqslant 0.5$ no ferromagnetic order was formed. For vacancy concentrations $x \geqslant 0.5$, the magnetic moment as a function of concentration can be seen in Fig. 7. Between $0.65 < x < 0.70$ a ferromagnetic onset occurs, with the magnetic

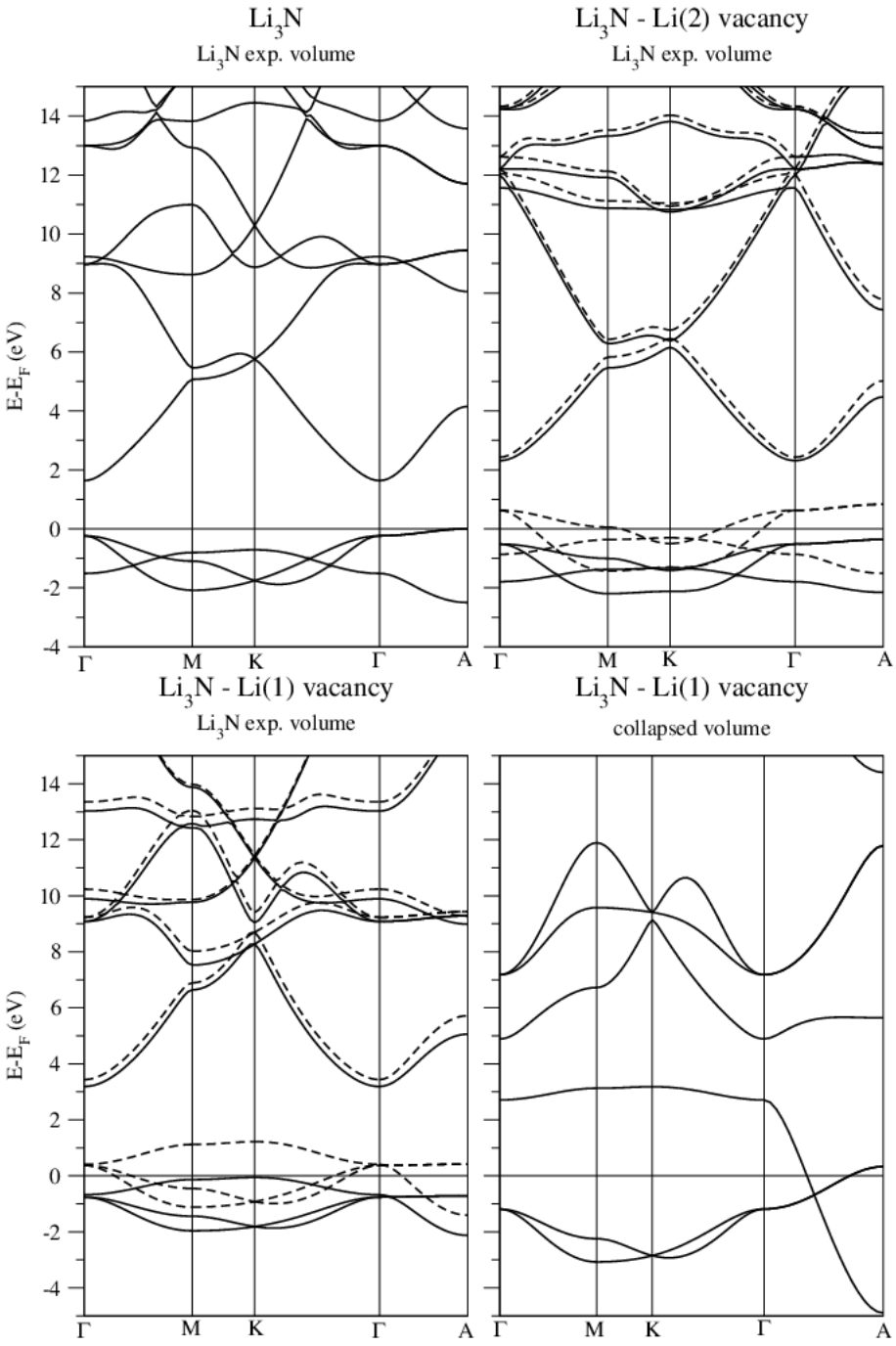

FIG. 6: Band structures. (Top left): Perfect $\alpha-Li_3N$. (Top right): Majority (full lines) and minority (dashed lines) bands for $\alpha-Li_3N$ with one fully vacated Li(2) atom. (Bottom left): Majority (full lines) and minority (dashed lines) bands for $\alpha-Li_3N$ with one fully vacated Li(1) atom. Evaluated at the experimental volume of perfect Li_3N. (Bottom right:) Bands for the volume collapsed Li_3N with fully vacated Li(1) atom.

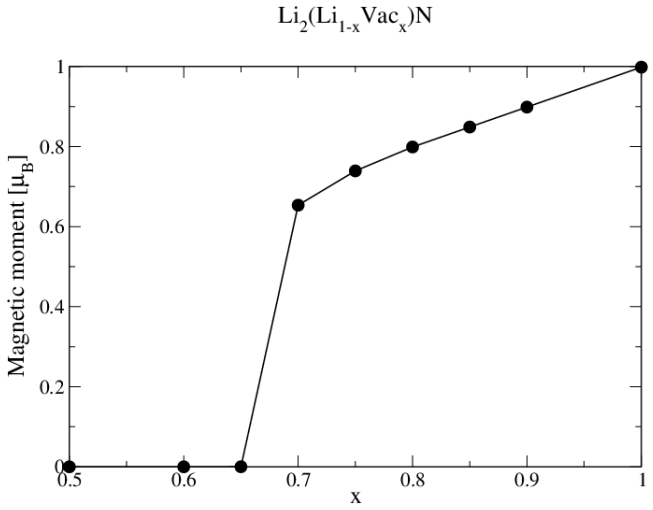

FIG. 7: Magnetic moment as function of concentration. Circles are actual calculated values, the solid lines are guides to the eye.

moment being proportional with vacancy concentration. At complete vacancy substitution the moment is $\sim 1\ \mu_B$.

In order to determine the ground state magnetic order present in the system, calculations assuming different antiferromagnetic (AFM) structures, as presented in Fig. 8, were performed. The antiferromagnetic supercells were calculated with the LMTO-ASA method [33]. Two configurations were investigated, see Fig. 8. One configuration with antiferromagnetic ordering *within* the basal $ab-$plane (AFI, Fig. 8 (left)), and one where the moments *between* the basal planes couple antiferromagnetically (AFII, Fig. 8 (right)).

For all studied AF structures, the total energies were higher than that of the FM solution (magnetic ground state configuration), but lower than the non-magnetic (NM) solution, $E_{FM} < E_{AFM} < E_{NM}$. For the AFM ordering with the moments alternating within the ab-plane (AFI, Fig. 8, left), the energy differences with respect to the ferromagnetic ground state is estimated to be $|\Delta E_{FM-AFM}| = 2.4$ mRy/atom (≈ 370 K). The non-magnetic state is situated at $|\Delta E_{FM-NM}| = 2.6$ mRy/atom (≈ 400 K) above the ferromagnetic groundstate. For the AFM ordering with the moments alternating between consecutive layers (AFII, Fig. 8, right) the energy difference was $|\Delta E_{FM-AFM}| = 0.24$ mRy (≈ 40 K), an order of magnitude smaller than the AFI configuration. Hence, coupling between neighbouring Li_2N layers can be considered negligible compared to the intralayer coupling.

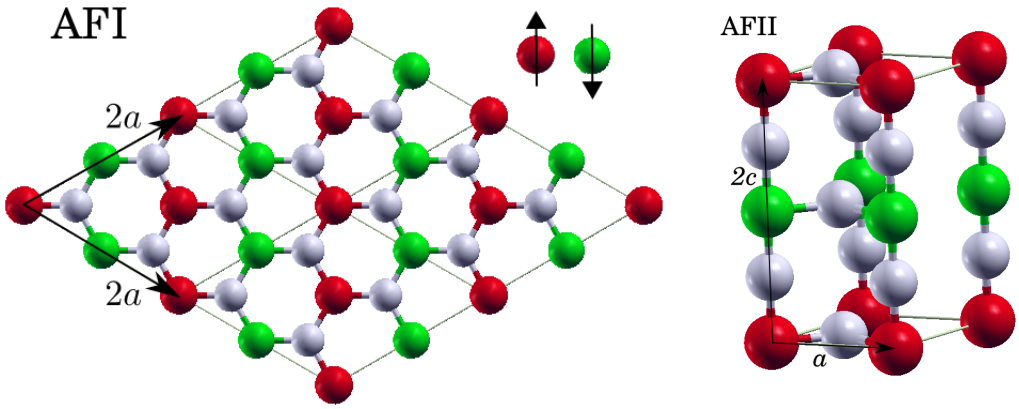

FIG. 8: AFI/II-type collinear magnetic state (left/right). The magnetic moment points along the $c-$axis; red (up); green (down). Grey spheres correspond to Li.

IV. DISCUSSION

Our results based on the DFT calculations show that the complete removal of one Li atom (in plane or between planes) triggers the magnetic moment formation, which is a consequence of the partial occupation of the N $p-$orbital. In the case of a full removal of the (out-of-plane) Li(1) atom, the crystal structure is unstable and undergoes a large reduction in volume. If one of the geometrically equivalent Li(2) atoms is removed, the volume reduction is much less drastic. To our best knowledge no experimental studies exist in which the full Li(2) vacancy has been achieved. On the other hand, one of the Li(2) positions has been vacated and in the same time the Li(1) atom has been fully substituted by Ni in the LiNiN structure [25, 26]. In this case, as expected the Ni $d-$bands are situated at the Fermi level, therefore the problem gain in complexity, as essentially correlation physics has to be included. Such calculations are outside the aims of the present study but shall be considered in a future work.

In our Li(2) vacated structure, the N binds 3 lithium ions within the basal plane. A similar local environment around the nitrogen is realized in the basal plane of $\beta-Li_3N$, which can be reached from $\alpha-Li_3N$ by applying modest pressure (~ 0.5 GPa) [22]. At this values of pressure, three of the six bonds of $\alpha-Li_3N$ are broken leading to 3 Li nearest neighbours around the N atom.

From our CPA calculations, the vacancy concentration leading to moment formation can be estimated. Early studies showed that the natural vacancy concentration of Li_3N is about

$1-2\%$ at the Li(2) positions, and that this does not change significantly with increasing temperature [40]. On the other hand, vacancies can also be created in a non-equilibrium situation, similarly to the one existing in battery cells where a voltage has been applied. The ionic conductivity will then remove Li from the system, and a larger concentration of vacancies may be achieved. Therefore, further experimental studies of magnetic properties as a function of vacancy concentration are desired to verify our theoretical estimations presented in this paper.

V. CONCLUSIONS

In this work we have performed density functional theory calculations for Li vacancies in $\alpha-Li_3N$. Assuming unchanged hexagonal crystal symmetry, and a complete removal of a Li(1) atom we showed by lattice relaxation that the unit cell volume and $c/a-$ratio will be drastically reduced and no magnetic moment is formed. By vacating the in-plane Li(2) atom for amounts larger than $> 65\%$ we predict that $\alpha-Li_3N$ can be turned metallic and ferromagnetic. The removal of a Li(2) atom will cause a less drastic structural reduction, and a magnetic ground state sets in with an ordered ferromagnetic moment of 1 μ_B.

ACKNOWLEDGEMENTS

The authors would like to acknowledge Anton Jesche for helpful discussions. The Deutsche Forschungsgemeinschaft through TRR80 is gratefully acknowledged for financial support. We acknowledge computational resources provided by the Swedish National Infrastructure for Computing (SNIC) at the National Supercomputer Centre (NSC) in Linköping.

---

[1] A. Rabenau and H. Schulz, Journal of the Less Common Metals **50**, 155159 (1976), ISSN 0022-5088, URL http://www.sciencedirect.com/science/article/pii/0022508876902630.

[2] A. Rabenau, Solid State Ionics **6**, 277293 (1982), ISSN 0167-2738, URL http://www.sciencedirect.com/science/article/pii/0167273882900121.

[3] H. Schulz and K. Schwarz, Acta Crystallographica Section A **34**, 9991005 (1978), URL http://dx.doi.org/10.1107/S0567739478002041.

[4] Tarascon J.-M. and Armand M., Nature **414**, 359367 (2001), ISSN 0028-0836.

[5] H. Brendecke and W. Bludau, Journal of Applied Physics **50**, 47434746 (1979), URL http://scitation.aip.org/content/aip/journal/jap/50/7/10.1063/1.326533.

[6] W. Sachsze and R. Juza, Z. Anorg. Allg. Chem. **259**, 278 (1949), ISSN 1521-3749, URL http://dx.doi.org/10.1002/zaac.19492590510.

[7] J. Klatyk, W. Schnelle, F. R. Wagner, R. Niewa, P. Novák, R. Kniep, M. Waldeck, V. Ksenofontov, and P. Gütlich, Phys. Rev. Lett. **88**, 207202 (2002), URL http://link.aps.org/doi/10.1103/PhysRevLett.88.207202.

[8] P. Novák and F. R. Wagner, Phys. Rev. B **66**, 184434 (2002), URL http://link.aps.org/doi/10.1103/PhysRevB.66.184434.

[9] V. P. Antropov and V. N. Antonov, Phys. Rev. B **90**, 094406 (2014), URL http://link.aps.org/doi/10.1103/PhysRevB.90.094406.

[10] Jesche A., McCallum R.W., Thimmaiah S., Jacobs J.L., Taufour V., Kreyssig A., Houk R.S., Budko S.L., and Canfield P.C., Nat. Commun. **5** (2014).

[11] A. Jesche, L. Ke, J. L. Jacobs, B. Harmon, R. S. Houk, and P. C. Canfield, Phys. Rev. B **91**, 180403 (2015), URL http://link.aps.org/doi/10.1103/PhysRevB.91.180403.

[12] P. Hohenberg and W. Kohn, Phys. Rev. **136**, B864 (1964).

[13] W. Kohn and L. J. Sham, Phys. Rev. **140**, A1133 (1965).

[14] W. Kohn, Rev. Mod. Phys. **71**, 1253 (1999).

[15] G. Kerker, Phys. Rev. B **23**, 6312 (1981), URL http://link.aps.org/doi/10.1103/PhysRevB.23.6312.

[16] P. Blaha, J. Redinger, and K. Schwarz, Z. Phys. B **57**, 273279 (1984), ISSN 1431-584X, URL http://dx.doi.org/10.1007/BF01470416.

[17] J. Sarnthein, K. Schwarz, and P. E. Blöchl, Phys. Rev. B **53**, 9084 (1996), URL http://link.aps.org/doi/10.1103/PhysRevB.53.9084.

[18] R. Dovesi, C. Pisani, F. Ricca, C. Roetti, and V. R. Saunders, Phys. Rev. B **30**, 972 (1984), URL http://link.aps.org/doi/10.1103/PhysRevB.30.972.

[19] M. Seel and R. Pandey, International Journal of Quantum Chemistry **40**, 461 (1991), ISSN 1097-461X, URL http://dx.doi.org/10.1002/qua.560400843.

[20] S. Wu, Z. Dong, F. Boey, and P. Wu, Appl. Phys. Lett. **94**, 172104 (2009), URL http://scitation.aip.org/content/aip/journal/apl/94/17/10.1063/1.3126449.

[21] H. J. Beister, S. Haag, R. Kniep, K. Strssner, and K. Syassen, Angewandte Chemie International Edition in English **27**, 1101 (1988), ISSN 1521-3773, URL http://dx.doi.org/10.1002/anie.198811011.

[22] A. Lazicki, B. Maddox, W. J. Evans, C.-S. Yoo, A. K. McMahan, W. E. Pickett, R. T. Scalettar, M. Y. Hu, and P. Chow, Phys. Rev. Lett. **95**, 165503 (2005), URL http://link.aps.org/doi/10.1103/PhysRevLett.95.165503.

[23] A. Lazicki, C. W. Yoo, W. J. Evans, M. Y. Hu, P. Chow, and W. E. Pickett, Phys. Rev. B **78**, 155133 (2008), URL http://link.aps.org/doi/10.1103/PhysRevB.78.155133.

[24] S. Wu, Z. Dong, P. Wu, and F. Boey, J. Mater. Chem. **21**, 165170 (2011), URL http://dx.doi.org/10.1039/C0JM01883J.

[25] M. G. Barker, A. J. Blake, D. H. Gregory, D. J. Siddons, S. E. Smith, P. P. Edwards, and T. A. Hamor, Chem. Commun. p. 11871188 (1999), URL http://dx.doi.org/10.1039/A902962A.

[26] Z. Stoeva, R. Gomez, D. H. Gregory, G. B. Hix, and J. J. Titman, Dalton Trans. pp. 3093–3097 (2004), URL http://dx.doi.org/10.1039/B401272K.

[27] P. Mohn, *Magnetism in the solid state* (Springer Verlag, Berlin, 2002).

[28] O. Volnianska and P. Boguslawski, Journal of Physics: Condensed Matter **22**, 073202 (2010), URL http://stacks.iop.org/0953-8984/22/i=7/a=073202.

[29] http://elk.sourceforge.net/.

[30] O. K. Andersen, O. Jepsen, and G. Krier, in *Lectures on Methods of Electronic Structure Calculations*, edited by V. Kumar, O. Andersen, and A. Mookerjee (World Scientific Publishing Co., Singapore, 1994), p. 63.

[31] L. Vitos, H. L. Skriver, B. Johansson, and J. Kollár, Comp. Mat. Sci. **18**, 24 (2000).

[32] L. Vitos, Phys. Rev. B **64**, 014107 (2001).

[33] O. K. Andersen, Phys. Rev. B **12**, 3060 (1975).

[34] J. Kollár, L. Vitos, and H. L. Skriver, in *Electronic Structure and Physical Properties of Solids: The Uses of the LMTO Method*, edited by H. Dreyssé (Lectures Notes in Physics (Springer-Verlag, Berlin), 2000), p. 85.

[35] L. Vitos, I. A. Abrikosov, and B. Johansson, Phys. Rev. Lett. **87**, 156401 (2001), URL http://link.aps.org/doi/10.1103/PhysRevLett.87.156401.

[36] J. P. Perdew and Y. Wang, Phys. Rev. B **45**, 13244 (1992).

[37] A. E. Kissavos, L. Vitos, and I. A. Abrikosov, Phys. Rev. B **75**, 115117 (2007), URL http://link.aps.org/doi/10.1103/PhysRevB.75.115117.

[38] J. P. Perdew, K. Burke, and M. Ernzerhof, Phys. Rev. Lett. **77**, 3865 (1996), URL http://link.aps.org/doi/10.1103/PhysRevLett.77.3865.

[39] A. Östlin and L. Vitos, Phys. Rev. B **84**, 113104 (2011), URL http://link.aps.org/doi/10.1103/PhysRevB.84.113104.

[40] H. Schulz and K. H. Thiemann, Acta Cryst. **35**, 309314 (1979), URL http://dx.doi.org/10.1107/S0567739479000632.